ADVANCING EARTH AND SPACE SCIENCES

Geophysical Research Letters

RESEARCH LETTER
10.1029/2025GL121318

Terrestrial Runoff Divides the Central Arctic Ocean and Shapes the Biologically Relevant Marine Lightscape

Håkon Sandven[1], David McKee[2], Rafael Gonçalves-Araujo[3], Rüdiger Röttgers[4], Anders F. Opdal[5], Philipp Assmy[6], and Mats A. Granskog[6]

[1]Department of Physics and Technology, University of Bergen, Norway and the Bjerknes Centre, Bergen, Norway, [2]Department of Physics, University of Strathclyde, Glasgow, UK, [3]National Institute of Aquatic Resources, Technical University of Denmark, Lyngby, Denmark, [4]Institute of Carbon Cycles, Helmholtz-Zentrum Hereon GmbH, Geesthacht, Germany, [5]Department of Biological Sciences, University of Bergen, Bergen, Norway, [6]Norwegian Polar Institute, Fram Centre, Tromsø, Norway

Key Points:

- Terrestrially sourced organic matter is a key factor controlling variability of light attenuation across the Nansen and Amundsen Basin
- Higher colored dissolved organic matter absorption in Transpolar Drift inhibits phytoplankton growth and may increase grazing pressure
- Phytoplankton govern variability of optical properties in the Atlantic water domain in the Nansen Basin

Supporting Information:

Supporting Information may be found in the online version of this article.

Correspondence to:

H. Sandven,
hakon.sandven@uib.no

Citation:

Sandven, H., McKee, D., Gonçalves-Araujo, R., Röttgers, R., Opdal, A. F., Assmy, P., & Granskog, M. A. (2026). Terrestrial runoff divides the Central Arctic Ocean and shapes the biologically relevant marine lightscape. *Geophysical Research Letters*, *53*, e2025GL121318. https://doi.org/10.1029/2025GL121318

Received 19 DEC 2025
Accepted 16 APR 2026

Abstract

The Arctic Ocean is undergoing drastic changes in its sea ice cover, but is also optically complex. Observations from summer 2022 across the western Eurasian Basin, show increased colored dissolved organic matter (CDOM) absorption from terrestrial-derived runoff within the Transpolar Drift (TPD) in the Amundsen Basin, extending down to a depth of ∼100 m. This is in stark contrast to the low-CDOM waters of the Atlantic-influenced Nansen Basin. The higher CDOM absorption increases the diffuse attenuation coefficient K_d by around 35% relative to Atlantic-influenced waters, and changes the spectral quality of light at depth. An irradiance model demonstrates that the decreased light availability can delay or inhibit under-ice phytoplankton blooms, affect zooplankton behavior, and cause enhanced solar heating in the upper 10 m. These findings show that simplified representations of light attenuation in present Earth System Models can hinder accurate assessments of light limitations on Arctic marine ecosystems.

Plain Language Summary

Climate change is rapidly transforming the Arctic Ocean through strong sea ice decline. These changes affect the amount of sunlight penetrating the ocean, which will have large effects on marine ecosystems. The Arctic Ocean is the smallest of the world oceans, yet receives a disproportionately large amount of terrestrial freshwater, propagating through the Central Arctic Ocean as the Transpolar Drift ocean current. Here, we present optical measurements from a research expedition in July 2022, conducted at different depths in the upper water column of the Central Arctic Ocean. We show that light absorption in the Transpolar Drift is driven by terrestrially derived dissolved organic matter, while absorption by phytoplankton is the dominant factor in the Atlantic-influenced waters closer to Svalbard. Using a light model, we show that increased light absorption by CDOM can postpone or inhibit the initiation of under-ice phytoplankton blooms in spring and potentially change the vertical distribution of solar heating in the water column. In addition, predators that rely on vision will struggle finding their prey, allowing zooplankton to migrate closer to the surface, and in turn increase the grazing pressure on phytoplankton. Crucially, these regional differences are not taken into account in most biogeochemical models.

1. Introduction

The Arctic Ocean is changing rapidly, with decreasing sea ice cover and increasing water temperatures induced by an Arctic warming four times the rate of the global average (Jahn et al., 2024; Rantanen et al., 2022). Accordingly, the foundation of Arctic marine ecosystems is changing due to increased light availability, warmer water temperatures and increased nutrient supplies due to stronger inflow of Atlantic water and increased terrestrial runoff (Ardyna & Arrigo, 2020). A key hydrographical feature of the Central Arctic Ocean (CAO) is the Transpolar Drift (TPD), a surface current crossing the CAO from the East Siberian and Laptev Seas to the outlets in the Fram Strait and Canadian Arctic Archipelago (Charette et al., 2020). It is highly influenced by Siberian river runoff and shelf processes, providing nutrients, carbon, and trace elements to the CAO and the northwestern Atlantic Ocean, and acts as a conveyor belt for sea ice (Kipp et al., 2018; Krumpen et al., 2019). Observations show significant amounts of colored dissolved organic matter (CDOM) within the TPD, affecting the underwater light environment and radiative heating (Gonçalves-Araujo et al., 2018; Granskog et al., 2015; Hill, 2008; Lund-Hansen et al., 2015; Pefanis et al., 2020). CDOM has a strong correlation with meteoric (runoff and precipitation) water fraction f_{mw}, enabling it to be used as an oceanographic tracer (Dodd et al., 2012; Petit et al., 2022; Stedmon

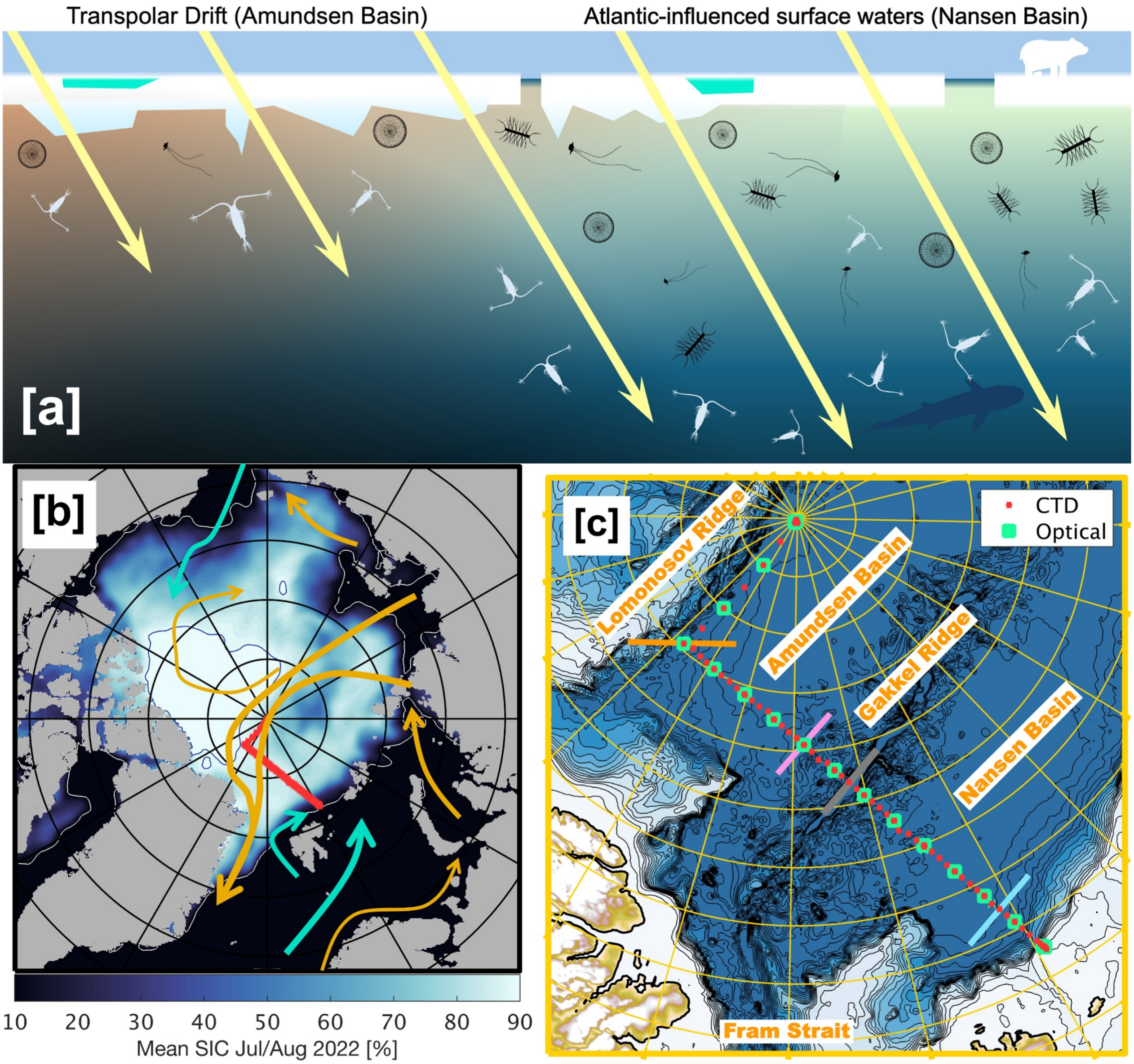

Figure 1. A diagram showing the hypothesized contrasts within the CAO (a), along with maps showing measurement locations of the AO2022 cruise. The average sea ice concentration (from ERA5/EUMETSAT OSI SAF) is shown (b), including major pathways of freshwater run-off (orange lines) and oceanic water inflow (teal lines). White lines indicate 10% SIC and dark blue lines indicate 90% SIC. Figure (c) shows the bathymetry (ETOPO2) of the region with CTD stations (red dots), optical stations (green squares), and colored lines refering to specific points on the transect, see Figure 2.

et al., 2015). Earlier work has shown that the elevated CDOM in the TPD is humic-like and thus of terrestrial origin (Charette et al., 2020; Stedmon et al., 2021; Wünsch et al., 2025).

The lightscape is the amount, spectral quality and diurnal variability of irradiance penetrating into the water column. It defines the euphotic zone (Figure 1a), the part of the ocean where daytime photosynthesis outbalances grazing losses and nighttime respiration such that net primary productivity can occur (Sakshaug & Slagstad, 1991). Grazing zooplankton also adjust to diurnal variability in light levels by vertical migration down to depths of several hundred meters, balancing their search for food with the risk of being eaten (Berge et al., 2014). The CAO is unique among the world oceans by having low diurnal variability of sunlight. Instead, an extreme seasonal variability dominates. Sea ice also impacts the underwater light environment tremendously, attenuating up to several orders of magnitude of light depending on snow and ice thickness and properties (e.g., Nicolaus et al., 2012; Stroeve et al., 2021). Melt ponds and open water areas (leads) are key features for transmitting light

10.1029/2025GL121318

into the ocean below (Light et al., 2015), enabling the development of large under-ice blooms in spring (e.g., Ardyna et al., 2020; Assmy et al., 2017). Cloud cover also reduces light penetrating into the ocean (albeit secondary to sea ice; Sandven et al., 2025), as well as particulate and dissolved matter in the water column (Park et al., 2015).

However, it is uncertain whether CAO annual primary production is light- or nutrient-limited, with a clear regional divide in the nutrient stoichiometries (Tremblay et al., 2015). Atlantic-influenced surface waters are enriched in nitrate relative to silicic acid and poor in the micronutrient iron, which limit Nansen Basin primary production (Rijkenberg et al., 2018). Conversely, the terrestrially derived freshwater is nitrate-CHL poor, causing nitrate limitation within the TPD (Liguori et al., 2021).

Measurements of inherent optical properties in the CAO water column are sparse, and most of the observational data sets in the region are from the adjacent shelf seas. The earliest published measurements are by Smith (1973) and Pegau (2002), the latter using the WetLabs ac-9 instrument profiling the upper 60 m of the water column in the Chukchi Sea. Stedmon et al. (2011) presented measurements of CDOM across the CAO and from Siberian rivers. Lund-Hansen et al. (2015) and Gonçalves-Araujo et al. (2018) published comprehensive data sets of CDOM and particulate absorption from the CAO, showing that the spatial variability of CDOM in surface waters of the CAO is largely driven by the presence or absence of TPD waters. Only a few studies exist concerning the optical scattering in the CAO (Gardner et al., 2022; Sandven et al., 2020), while the shelf areas have been studied more extensively (e.g., Bélanger et al., 2013; Matsuoka et al., 2011; Reynolds et al., 2016; Sandven et al., 2023). Satellite ocean color observations are scarce in the Arctic due to the persistent ice and cloud cover (Castro de la Guardia et al., 2023).

This study presents a unique data set with depth-resolved optical properties along a transect in the western Eurasian basin of the CAO traversing hydrographically and optically contrasting surface waters in the TPD-influenced Amundsen Basin and the Atlantic-influenced Nansen Basin. A hyperspectral light field model is used to assess the effect of contrasting optical properties across the region on the underwater light environment.

2. Methods

2.1. Field Campaign

Measurements were conducted during the Arctic Ocean 2022 (AO2022) cruise onboard RV Kronprins Haakon (Dodd, Nikolopoulos, et al., 2022). The transect started at the North Pole on July 29, and ended on August 19 at the continental slope northeast of Svalbard, see (Figures 1b and 1c). The methods and observational products are described in detail in Supporting Information S1.

Key optical measurements included CDOM and particulate light absorption coefficients ($a_{\mathrm{CDOM}}(\lambda)$ and $a_{\mathrm{p}}(\lambda)$, shown for wavelengths of 400 and 440 nm) from water samples, using well-established methodology (Neeley & Mannino, 2018; Röttgers et al., 2016; Röttgers & Gehnke, 2012). In situ profiles of non-water absorption $a_{\mathrm{nw}}(\lambda)$ and attenuation $c_{\mathrm{nw}}(\lambda)$ were recorded with an ac-s instrument (Seabird Sci.; Moore et al., 1997; Röttgers et al., 2013). Chl *a* fluorescence measurements made with the WET Labs ECO-FL fluorometers from the ship-CTD were cross-calibrated using chl *a* concentration measurements from water samples (Figure S1 in Supporting Information S1). Salinity and oxygen isotope ratios δ^{18}O from water samples were used to derive the meteoric water fraction f_{mw} and the fraction of sea ice meltwater f_{SIM} (Bauch et al., 1995; Dodd et al., 2012). Accompanying measurements included salinity and temperature profiles from the ship-CTD (Dodd, Buckley, et al., 2022).

We use Kendall's τ for statistical analysis throughout, given the lack of normality or linearity in many of the bio-optical relationships.

2.2. Lightscape Modelling

We use the hyperspectral irradiance model HEIMDALL (Connan-McGinty et al., 2022) to model how CDOM alters the marine lightscape and thereby affects primary and secondary productivity (Figure 1a). HEIMDALL has been used in several studies to study how light availability affects various trophic levels in Arctic waters (Häfker et al., 2022; Sandven et al., 2025; Schartmüller et al., 2023).

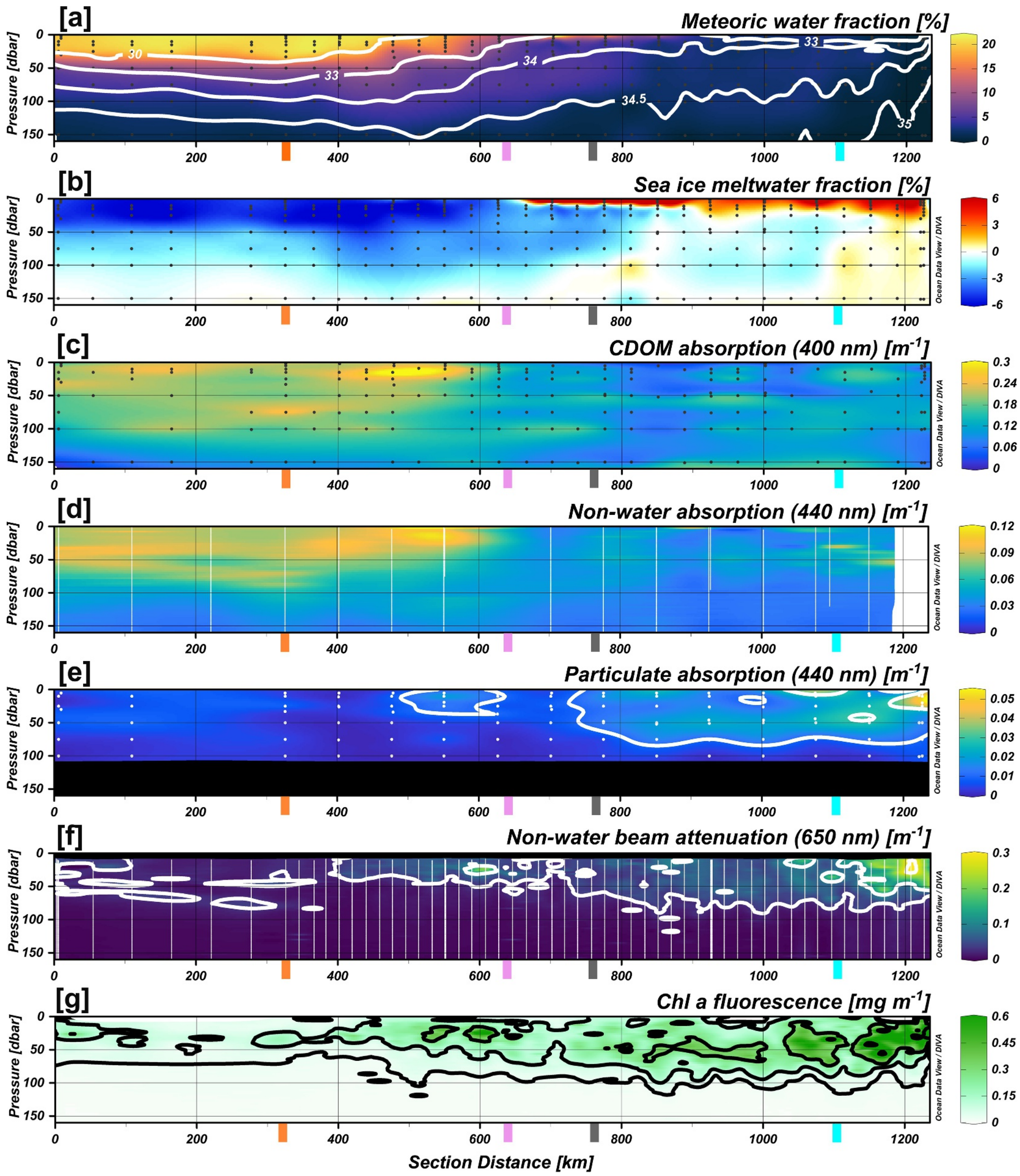

Figure 2. Transect from the 2022 cruise, starting from the left at the North Pole and ending just outside the ice edge northeast of Svalbard, see Figure 1. Along the *x*-axis of the panels, orange lines indicate the 90° turn in the transect, pink lines show roughly the extent of the TPD, charcoal lines indicate the Gakkel Ridge, and the approximate sea ice edge is illustrated with turquoise lines. Transects of (a) meteoric water and (b) sea ice meltwater fractions are shown (black dots show sampling locations/depths), with salinity shown as isolines in (a). (c) Measurements of $a_{\mathrm{CDOM}}(400\ \mathrm{nm})$ from water samples. (d) Non-water absorption coefficients (ac-s instrument) at 440 nm, with white vertical lines showing the stations. (e) $a_p(440\ \mathrm{nm})$. (f) Non-water beam attenuation coefficient at 650 nm, with white vertical lines indicating the CTD casts. (g) Corrected in situ Chl *a* fluorescence. In Figures 2e–2g, the plotted isolines correspond to values 0.03, 0.1, 0.3, and 1 to highlight variability in the lower data range.

Incoming light $E_0(\lambda)$ is computed based on solar zenith angle, lunar phase and zenith angle, and total cloud cover from ERA5 (Hersbach et al., 2020). Transmitted light is estimated by weighing the transmittance of sea ice (including snow) and open-water, with the sea ice concentration provided by EUMETSAT (Lavergne et al., 2019). Transmittance of (snow-covered) sea ice is estimated using spectral $K_D(\lambda)$ and albedo for snow and sea ice, together with estimates of snow depth and ice thickness (PIOMAS; Zhang & Rothrock, 2003). The methodology is detailed in Connan-McGinty et al. (2025) and Sandven et al. (2025). The underwater irradiance levels $E_d(z,\lambda)$ are thereafter calculated with diffuse and direct light attenuation coefficients derived from bio-optical relationships. This approach has been validated using glider observations of $E_{\mathrm{PAR}}(z)$ in the Barents Sea (Connan-McGinty et al., 2022).

For simplicity, we assume zero chl *a* absorption throughout the modeling component, and set fixed CDOM absorption spectra for a low and high f_{mw} based on field measurements (see Figure 3). In Figure 3, we demonstrate that chl *a* has a low impact on light attenuation compared to CDOM. Further, we focus mainly on the spring months before the phytoplankton self-shading may become a significant factor.

For the irradiance response of zooplankton, we follow the spectral weighting routine derived in Cohen et al. (2015), where we compute the utilized photons $E_{\mathrm{UP}}(z)$ by animals following the expression,

$$E_{\mathrm{UP}}(z) = \int_{400\mathrm{nm}}^{700\mathrm{nm}} E_d(z,\lambda) \cdot S(\lambda)\,\mathrm{d}\lambda.$$

Here, $S(\lambda)$ is the spectral sensitivity of krill or zooplankton. The shortwave radiative heating rate in the water column is estimated using Gershun's law:

$$H_{\mathrm{rad}}^{\mathrm{PAR}}(z) = \int_{400\mathrm{nm}}^{700\mathrm{nm}} E_d(z,\lambda) \cdot a_{\mathrm{tot}}(\lambda)\,\mathrm{d}\lambda,$$

where $a_{\mathrm{tot}}(\lambda)$ is the total absorption coefficient.

3. Results

3.1. Spatial Contrasts

Surface waters along the transect (Figure 2) can be divided into two distinctive regimes from a hydrographical, optical and biogeochemical point of view. The part affected by the TPD starts at the North Pole and ends after ~650 km near 86°N, 0°E (pink lines), and is characterized by high f_{mw}, low salinity (29–33), and negative f_{SIM}. The latter implies that this water fraction has been rejected as brine during sea ice formation (likely driving vertical mixing), and is prevalent in the CAO and the Fram Strait water column (Dodd et al., 2012; Laukert et al., 2025). There is relatively high absorption at 440 nm, which follow the spatial pattern of TPD as well as $a_{\mathrm{CDOM}}(400\ \mathrm{nm})$, with some discrepancies due to spatial interpolation. The TPD and Amundsen Basin overlap reasonably well in geographical extent, however the TPD can be highly variable (Wilson et al., 2021).

Outside the TPD, $a_{\mathrm{CDOM}}(400\ \mathrm{nm})$ and $a_{\mathrm{nw}}(440\ \mathrm{nm})$ are generally low ($a_{\mathrm{nw}} < 0.05\ \mathrm{m}^{-1}$), with the surface halocline associated with seasonal sea ice meltwater. Increases in absorption are driven by $a_{\mathrm{p}}(\lambda)$, see Figure 2e. We find elevated chl *a* fluorescence (>0.5 mg m^{-1}; Figure 2h) corresponding well with $a_{\mathrm{p}}(440\ \mathrm{nm})$ increases, while $a_{\mathrm{nw}}(440\ \mathrm{nm})$ increases with both higher a_{CDOM} and chl *a*. In contrast, the spatial structure of the non-water beam attenuation $c_{\mathrm{nw}}(650\ \mathrm{nm})$ follows chl *a* and not the CDOM absorption. We see lower chl *a* fluorescence in the TPD than in the Nansen Basin, and a shallower deep chlorophyll maxima than further south. There is a strong increase near the sea ice edge where warm Atlantic water enters the CAO from the Fram Strait. Note that the horizontal extent of features can easily be exaggerated by the interpolation algorithm (weighted-average gridding) in the plotting software (ODV; Schlitzer, 2022). Absolute values should be used with care.

3.2. Drivers of Optical Variability

In Figure 3a, the relationship between chl *a* and $a_{\mathrm{p}}(440\ \mathrm{nm})$ is shown together with corresponding relationships from the global ocean (Bricaud et al., 1998) and an under-ice phytoplankton spring bloom north of Svalbard (Pavlov et al., 2017). Measurements from the NOMAD (Werdell & Bailey, 2005) and COASTℓOOC (Massicotte et al., 2023a, 2023b) data sets are also shown, spanning the global ocean and European coastal waters, respectively. We see a high correlation ($\tau = 0.67$), and similar spread in our data set as the reference measurements, albeit with low agreement for the smallest chl *a* values where measurement uncertainties are high. The chl *a* specific absorption inferred from regression of our data set is lower than in the global data sets, but consistent with results from ice-covered waters (e.g., Pavlov et al., 2017; Sandven et al., 2023), which could be due to low-light acclimated communities. Chl *a* is also significantly correlated with scattering, see Figure S1C in Supporting Information S1 ($\tau = 0.69$ with beam attenuation at 650 nm, where CDOM influence is minimal).

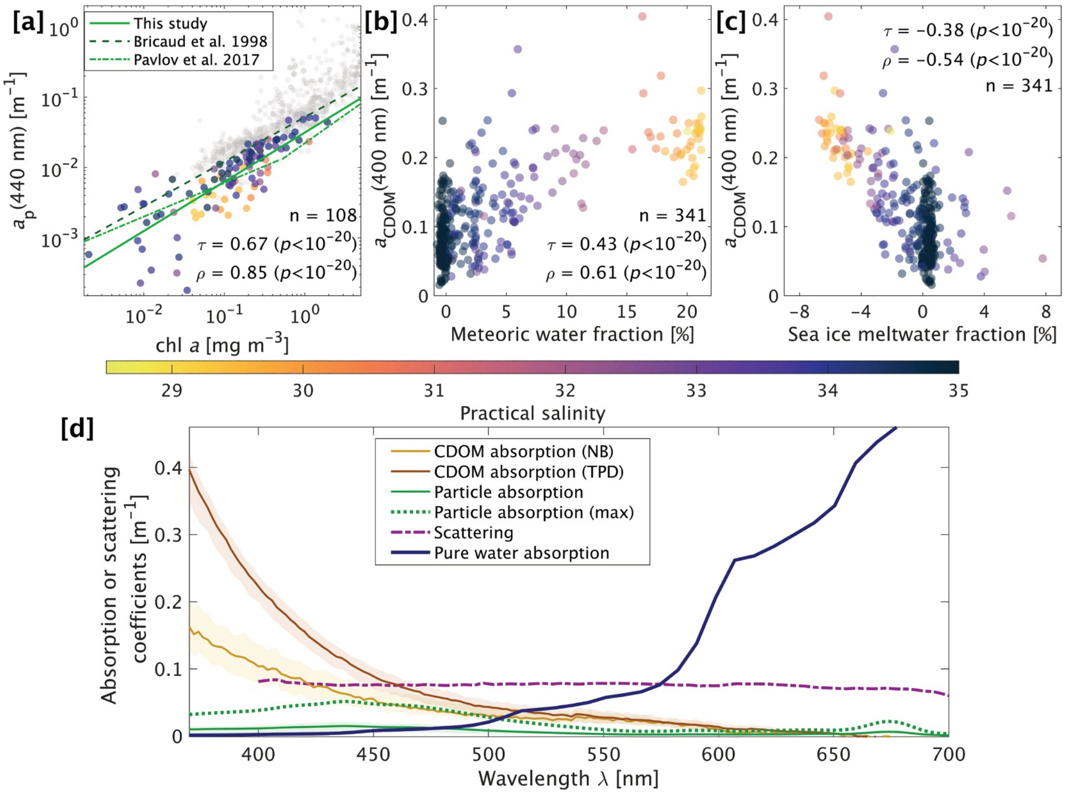

Figure 3. Relationships showing optical variability and how it is driven by biogeochemical properties. (a) Measure $a_p(440\text{ nm})$ as a function of chl *a* and salinity (color bar), including results from earlier studies in ice-covered and open waters for context (gray dots). Relationship between (b) meteoric water fraction and $a_{\text{CDOM}}(400\text{ nm})$ (c) sea ice meltwater fraction and $a_{\text{CDOM}}(400\text{ nm})$. Correlation coefficients Kendall's τ and Spearman's ρ are shown. (d) Spectral comparison between parsed components of the inherent optical properties in the upper 50 m of the water column. Colored dissolved organic matter absorption for the Nansen Basin (NB, defined as $f_{\text{mw}} < 2$) and in the TPD ($f_{\text{mw}} > 10$) is shown as yellow and brown lines respectively (shaded areas are the quartiles). Particulate absorption is similarly shown in green, with the maximum absorption spectrum shown as a green dotted line. The average scattering spectrum (derived from ac-s measurements) is shown as a purple dashed-dotted line, and the pure water absorption as a solid dark blue line (from Pope & Fry, 1997).

CDOM absorption is closely linked to terrestrial runoff, as shown in Figure 3b, and dominates the absorption budget at shorter wavelengths (Figure 3d), demonstrating the optical complexity of TPD. The correlation between $a_{\text{CDOM}}(400\text{ nm})$ and f_{mw} ($\tau = 0.43$, corresponding to $r \approx 0.6$) is not particularly strong, but improves at shorter wavelengths ($\tau = 0.56$ for $a_{\text{CDOM}}(350\text{ nm})$) and worsens at longer wavelengths ($\tau = 0.32$ for $a_{\text{CDOM}}(440\text{ nm})$). This implies that a_{CDOM} measurement uncertainties, which are challenging at low concentrations, may have a strong impact. However, the linear mixing model is not straightforward to interpret (Laukert et al., 2025), and higher $a_{\text{CDOM}}(\lambda)$ has a negative linear relationship with sea ice meltwater ($\tau = -0.38$; Figure 3c), driven mainly by brine. The correlation of $a_{\text{CDOM}}(400\text{ nm})$ with salinity is $\tau = -0.43$ (see also Figure S2 in Supporting Information S1).

While pure water absorption dominates in the red part of the spectrum, suspended particulate matter only has a weak influence on the light attenuation (Figure 3d). The diffuse attenuation coefficient is often modelled as the sum of the absorption and backscattering coefficients, and the latter is typically only ~2% of the scattering coefficient, meaning that particulate scattering has a negligible contribution. Nonetheless, the phytoplankton concentrations during spring blooms can easily be more than an order of magnitude higher than our late summer observations (Assmy et al., 2017) and thus much more optically important within the bloom periods. Under-ice spring blooms are typically dominated by diatoms or the haptophyte algae *Phaeocystis* (Ardyna et al., 2020; Assmy et al., 2017; Sherr et al., 2003). *Phaeocystis* blooms cause an increase in scattering-to-absorption ratio driven by their size and structure (Pavlov et al., 2017). Including phytoplankton will increase the accuracy of the irradiance modeling, but requires year-round vertically resolved observations or highly uncertain estimates from modelling.

4. Lightscape Effects

How does the increased CDOM absorption in the TPD affect the under-ice light environment? Results from the HEIMDALL model (Figure 4) illustrate how CDOM reduces light availability at biologically relevant depths throughout the productive season May-September. The location used in the modelling, 86.5°N 5°W, is near the edge of the TPD (pink line in Figure 2). Following Sverdrup's critical depth hypothesis (Sverdrup, 1953), the initiation of net primary productivity is associated with the light levels at the mixed layer depth surpassing a certain threshold (averaged over several days), called the compensation irradiance E_{PAR}. In ice-covered waters, the compensation irradiance is estimated as $E_{\mathrm{PAR}} = 0.25$ μmol m^{-2} s^{-1} (Randelhoff et al., 2020). Given that the mixed layer depth seasonality is unknown, we show the E_{PAR} isolume depth in Figure 4b to showcase the potential CDOM-induced delay. However, as discussed in Sandven et al. (2025), the phytoplankton compensation irradiance is subject to large uncertainties, and has not been estimated for the CAO. Vertical mixing is another important process (Lowry et al., 2018). For zooplankton, we use $E_{\mathrm{UP}} = 10^{-2}$ μmol m^{-2} s^{-1} as a threshold, following Häfker et al. (2022) for daytime values.

In May-June, the incoming solar irradiance is approaching its near-maximum (Figure 4a), however, the sea ice and snow layers (Figure 4b) are also thickest in May. Small leads formations can then have large impact on the under-ice lightscape. In July, the SIC decreased to ∼80%, leading to consistently deep isolume depths (after averaging the results across 4 days), varying tens of meters depending on a_{CDOM}. The ratio of $E_{\mathrm{PAR}}(z)$ inside and outside the TPD is plotted in Figure 4e (green lines), roughly following an exponential decrease. The approximate K_d(PAR) increases by ∼35% from 0.070 ±0.002 to 0.094 ±0.002 m^{-1}, and E_{PAR} at 40 m is reduced by about 60%. This reduction may therefore play a crucial role in the initation of under-ice phytoplankton blooms, postponing it up to several weeks depending on the mixed layer depth and wind mixing (see also Figure S3 in Supporting Information S1 for average over the period 2003–2022). This is corroborated by the transects in Figure 2, where we see an increase in chl *a* concentration and a distinctly deeper productive layer as we move east from the Amundsen Basin to the Nansen Basin. We neglect the phytoplankton self-shading, as Figure 3d shows that the effect is minimal compared to CDOM.

Further complexity is added when considering spectral effects, see Figure 4d. Disregarding spectral dependencies has been shown to introduce large errors in modelled chl *a* and primary production (Bouman et al., 2020; Mobley et al., 2015). CDOM absorbs more blue light than green and red, which shifts the underwater light spectrum towards a larger fraction of green light. This can impact biodiversity among both primary producers and higher trophic levels (Soja-Woźniak et al., 2025; Utne-Palm, 1999).

In many parts of the world ocean, zooplankton migrate vertically with the diurnal light cycle, but this pattern breaks down seasonally in the CAO with the lack of diel variability (Flores et al., 2023). It is partially replaced with the lunar cycle in winter (Last et al., 2016) and tidal cues in summer (Hüppe et al., 2020). Considering the realized daytime isolume from Häfker et al. (2022), we see that higher CDOM absorption in the TPD shifts the estimated zooplankton summer habitat upwards from >100 to ∼75 m. This implies a shoaling of zooplankton in the Amundsen Basin, but relevant observations are sparse (Ingvaldsen et al., 2023). Considering the cumulative lightscape pressure, higher light attenuation will potentially also decrease the predation risk of the secondary producers, leading to higher grazing pressure on phytoplankton. Synchrony of zooplankton and phytoplankton phenology is also important for trophic-level interactions (Renaud et al., 2024).

In Figure 4e, we show the ratio for the shortwave radiative heating rate $H_{\mathrm{rad}}^{\mathrm{PAR}}(z)$ within the visible spectra. Increased CDOM leads to higher heating rates near the surface and less heat being deposited at depth, as shown by the ratio for the radiative heating rate. Pefanis et al. (2020) demonstrated that this can lead to faster sea ice melt rates. The seasonal variability (Figure 4f) shows that the radiative heating mainly occurs in June-August when SIC < 90%. Our findings are roughly consistent with earlier studies in other parts of the Arctic Ocean (Granskog et al., 2015; Hill, 2008), but the CDOM effect is lower due to the higher SIC. Hence, CDOM-induced heating will likely become more important as the sea ice declines. While we do not include $H_{\mathrm{rad}}^{\mathrm{PAR}}(z)$ above 700 nm, this does not significantly affect the calculations since this radiation is mostly absorbed in the surface microlayer.

5. Conclusion

Light limitation confines the vertical and seasonal boundaries of primary productivity and affects grazing, while nutrient availability, wind mixing and stratification further determine primary production. Within the TPD, we

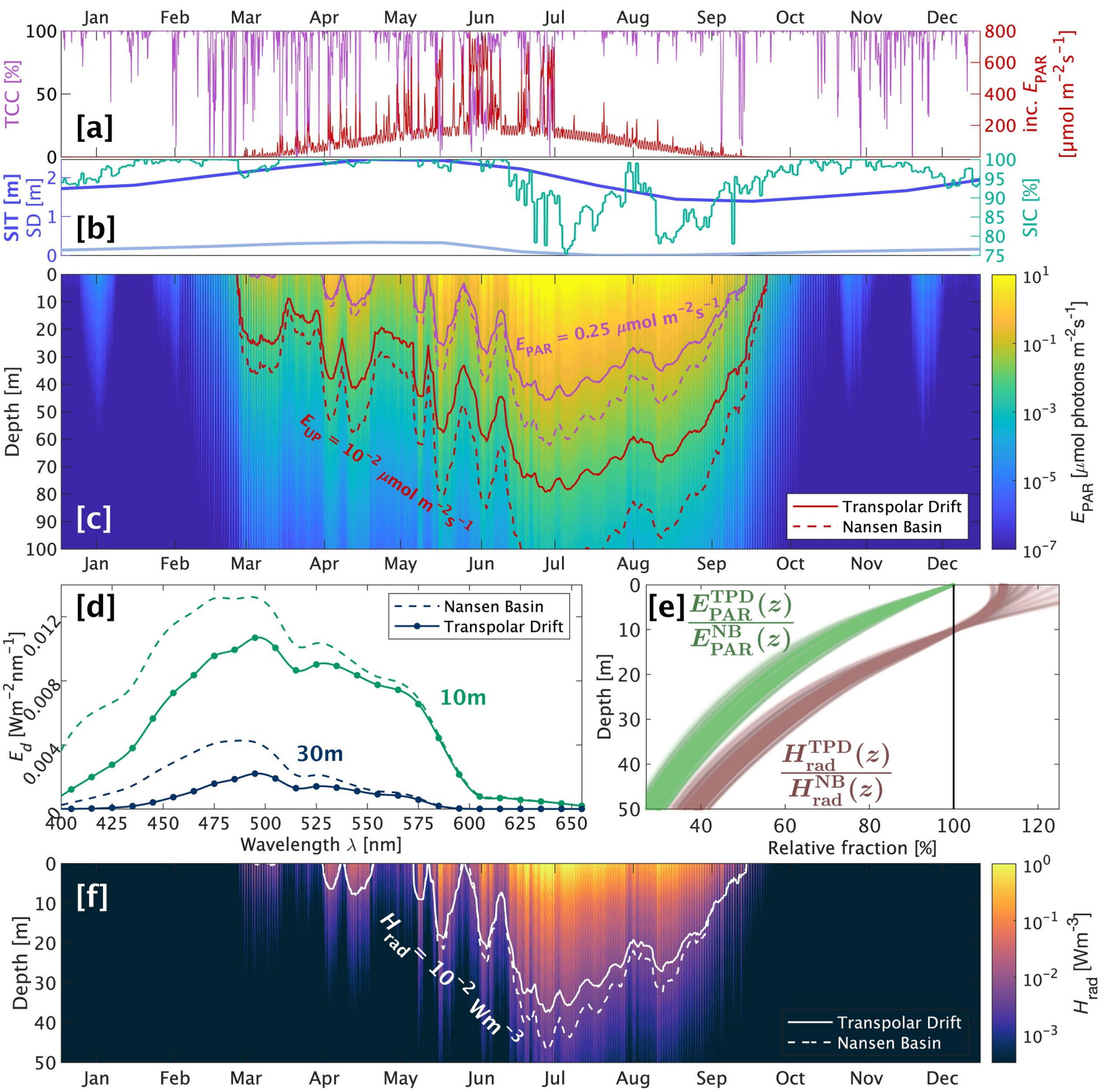

Figure 4. Results of hyperspectral irradiance modelling throughout 2022 at 86.5°N, 5°W, using 3h time resolution. (a) Model inputs (SIC and total cloud cover) from ERA5/EUMETSAT OSI-SAF together with the incoming surface E_{PAR}. (b) Model inputs (SIT and SD) from PIOMAS. (c) Simulated $E_{\mathrm{PAR}}(z)$. Red contour shows the phytoplankton-specific $E_{\mathrm{PAR}} = 0.25\ \mu\mathrm{mol\ m^{-2}\ s^{-1}}$ isolume depth, while the purple indicates the $E_{\mathrm{UP}} = 10^{-2}\ \mu\mathrm{mol\ m^{-2}\ s^{-1}}$ isolume depth characteristic for zooplankton daytime-habitat, both smoothed using a 4-day moving average. Dashed lines are for low colored dissolved organic matter (CDOM) absorption, characteristic of Nansen basin surface waters, and solid lines are with higher CDOM absorption characteristic of TPD (as shown in Figure 3d). (d) Variations in the irradiance spectrum at 10 and 30 m (average for July 2022), with a similar partition based on CDOM absorption. (e) Ratio of $E_{\mathrm{PAR}}(z)$ inside and outside the TPD (green lines) and heating rates $H_{\mathrm{rad}}(z)$ from visible radiation (red lines). (f) Variability in $H_{\mathrm{rad}}^{\mathrm{PAR}}(z)$ across 2022, with the isoline corresponding to $H_{\mathrm{rad}}^{\mathrm{PAR}} = 0.01\ \mathrm{Wm^{-2}}$. Similarly to Figure 4c, the dashed (solid) lines show outside (inside) the TPD.

find higher CDOM absorption, which has its origin primarily from Siberian rivers, supported by the presence of humic-like CDOM (Wünsch et al., 2025). In the Atlantic-influenced Nansen Basin, phytoplankton drives the optical variability, similar to the adjacent Barents Sea and Yermak Plateau (Kowalczuk et al., 2019; Sandven et al., 2023), and in most oceanic waters globally (Bricaud et al., 1998).

We know little about the seasonal and inter-annual development of the TPD and consequently its optical variability. Given that the TPD affects hydrography and optical properties down to ~100 m, well below the euphotic zone, the lightscape is highly sensitive to CDOM absorption, and high-accuracy optical measurements should be repeated at different times of the year, which can be linked to stationary or drifting observations of FDOM, chl *a* fluorescence and salinity. Haine et al. (2015) estimated the freshwater runoff into the CAO to increase by ∼30% by 2100, meaning CDOM variability is important for modelling future Arctic ecosystems, when we may get even stronger regional contrasts than today.

To better estimate the under-ice lightscape, we need better parametrizations for sea ice, snow and water column, which all also encompass large uncertainties in their large-scale products (Stroeve et al., 2021; Wilson et al., 2021). Using broadband diffuse attenuation coefficients characteristic of CDOM-rich waters ($K_d(\mathrm{PAR}) = 0.12\ \mathrm{m}^{-1}$) modelling studies (Clement Kinney et al., 2023; Horvat et al., 2017) have concluded that under-ice blooms have been relatively uncommon in the CAO, and to a large extent driven by advection from ice-free areas. Our study estimate $K_d(\mathrm{PAR})$ to span 0.070–0.094 m^{-1} in the CAO, depending on the f_{mw}, meaning that the under-ice light availability has likely been underestimated in these studies. Further, primary productivity varies significantly with diurnal cycle in addition to the 24-hr average (Mobley et al., 2015), meaning that lower latitude models cannot be translated directly to the high Arctic. There are still relatively few published observations of the initiation of spring productivity (Boles et al., 2020; Hoppe et al., 2024). Given the rapid ongoing changes, we urgently need to better understand the biological phenology and productivity underneath the sea ice cover to prepare for the future Arctic.

Conflict of Interest

The authors declare no conflicts of interest relevant to this study.

Availability Statement

The hydrographic and biogeochemical data used here is available as Dodd, Buckley, et al. (2022). The optical measurements used in the study is available as Sandven, Granskog, and Hamre (2026) and Sandven, Gonçalves-Araujo, et al. (2026). HEIMDALL modelling data and the CDOM spectra used in Figure 4 is available at Zenodo (Sandven, McKee, et al., 2026). The sea ice and cloud concentration used in the study are publicly available from the Copernicus Climate Data Store (Copernicus Climate Change Service, 2023). PIOMAS data is provided by the Polar Science Center, Applied Physics Laboratory, University of Washington, USA (https://psc.apl.uw.edu/research/projects/arctic-sea-ice-volume-anomaly/data/). The COASTℓOOC data set is available on SEANOE (Massicote et al., 2023a, 2023b), while the NOMAD data set is available on SeaBASS (https://seabass.gsfc.nasa.gov/wiki/NOMAD).

Acknowledgments
We thank the captain and the crew of R/V Kronprins Haakon for their support and assistance throughout the research cruise. Many thanks also to Megan Lenss for conducting the chl *a* water sample measurements, and to other cruise participants who have supported the data collection. The study received support from Shaping European Research Leaders for Marine Sustainability (SEAS) project, funded by the European Union's Horizon 2020 Framework Programme for Research and Innovation under the Marie Skłodowska-Curie Grant 101034309, the Research Council of Norway through the project The Nansen Legacy (Grant 276730) and PELAGIC (Grant 334996), the Fram Centre project Sustainable Development of the Arctic Ocean (SUDARCO, 2551323), and the Independent Research Fund Denmark (Grant 4251-00058B). The ship-time of the expedition was provided by the Norwegian Polar Institute.

References

Ardyna, M., & Arrigo, K. R. (2020). Phytoplankton dynamics in a changing Arctic Ocean. *Nature Climate Change*, *10*(10), 892–903. https://doi.org/10.1038/s41558-020-0905-y

Ardyna, M., Mundy, C. J., Mills, M. M., Oziel, L., Grondin, P. L., Lacour, L., et al. (2020). Environmental drivers of under-ice phytoplankton bloom dynamics in the Arctic Ocean. *Elementa: Science of the Anthropocene*, *8*, 30. https://doi.org/10.1525/elementa.430

Assmy, P., Fernández-Méndez, M., Duarte, P., Meyer, A., Randelhoff, A., Mundy, C. J., et al. (2017). Leads in Arctic pack ice enable early phytoplankton blooms below snow-covered sea ice. *Scientific Reports*, *7*(1), 40850. https://doi.org/10.1038/srep40850

Bauch, D., Schlosser, P., & Fairbanks, R. G. (1995). Freshwater balance and the sources of deep and bottom waters in the Arctic Ocean inferred from the distribution of H218O. *Progress in Oceanography*, *35*(1), 53–80. https://doi.org/10.1016/0079-6611(95)00005-2

Bélanger, S., Cizmeli, S. A., Ehn, J., Matsuoka, A., Doxaran, D., Hooker, S., & Babin, M. (2013). Light absorption and partitioning in Arctic Ocean surface waters: Impact of multiyear ice melting. *Biogeosciences*, *10*(10), 6433–6452. https://doi.org/10.5194/bg-10-6433-2013

Berge, J., Cottier, F., Varpe, Ø., Renaud, P. E., Falk-Petersen, S., Kwasniewski, S., et al. (2014). Arctic complexity: A case study on diel vertical migration of zooplankton. *Journal of Plankton Research*, *36*(5), 1279–1297. https://doi.org/10.1093/plankt/fbu059

Boles, E., Provost, C., Garçon, V., Bertosio, C., Athanase, M., Koenig, Z., & Sennéchael, N. (2020). Under-ice phytoplankton blooms in the central Arctic Ocean: Insights from the first biogeochemical IAOOS platform drift in 2017. *Journal of Geophysical Research: Oceans*, *125*(3), e2019JC015608. https://doi.org/10.1029/2019JC015608

Bouman, H. A., Jackson, T., Sathyendranath, S., & Platt, T. (2020). Vertical structure in chlorophyll profiles: Influence on primary production in the Arctic Ocean. *Philosophical Transactions of the Royal Society A*, *378*(2181), 20190351. https://doi.org/10.1098/rsta.2019.0351

Bricaud, A., Morel, A., Babin, M., Allali, K., & Claustre, H. (1998). Variations of light absorption by suspended particles with chlorophyll a concentration in oceanic (case 1) waters: Analysis and implications for bio-optical models. *Journal of Geophysical Research*, *103*(C13), 31033–31044. https://doi.org/10.1029/98JC02712

Castro de la Guardia, L., Fariñas, T. H., Marchese, C., Amargant-Arumí, M., Myers, P. G., Bélanger, S., et al. (2023). Assessing net primary production in the northwestern Barents Sea using in situ, remote sensing and modelling approaches. *Progress in Oceanography*, *219*, 103160. https://doi.org/10.1016/j.pocean.2023.103160

Charette, M. A., Kipp, L. E., Jensen, L. T., Dabrowski, J. S., Whitmore, L. M., Fitzsimmons, J. N., et al. (2020). The transpolar drift as a source of riverine and shelf-derived trace elements to the central Arctic Ocean. *Journal of Geophysical Research: Oceans*, *125*(5), e2019JC015920. https://doi.org/10.1029/2019JC015920

Clement Kinney, J., Frants, M., Maslowski, W., Osinski, R., Jeffery, N., Jin, M., & Lee, Y. J. (2023). Investigation of under-ice phytoplankton growth in the fully-coupled, high-resolution Regional Arctic System Model. *Journal of Geophysical Research: Oceans*, *128*(9), e2022JC019000. https://doi.org/10.1029/2022jc019000

Cohen, J. H., Berge, J., Moline, M. A., Sørensen, A. J., Last, K., Falk-Petersen, S., et al. (2015). Is ambient light during the high Arctic polar night sufficient to act as a visual cue for zooplankton? *PLoS One*, *10*(6), e0126247. https://doi.org/10.1371/journal.pone.0126247

Connan-McGinty, S., Banas, N. S., Berge, J., Cottier, F., Grant, S., Johnsen, G., et al. (2022). Midnight sun to polar night: A model of seasonal light in the Barents Sea. *Journal of Advances in Modeling Earth Systems*, *14*(10), e2022MS003198. https://doi.org/10.1029/2022MS003198

Connan-McGinty, S., Sandven, H., Banas, N. S., Röttgers, R., & Mckee, D. (2025). Advancing the HEIMDALL model: Seasonal spectral irradiance through the Pan-Arctic icescape. *Authorea Preprints*. https://doi.org/10.22541/essoar.173991250.05381697/v1

Copernicus Climate Change Service, Climate Data Store. (2023). ERA5 hourly data on single levels from 1940 to present [Dataset]. *Copernicus Climate Change Service (C3S) Climate Data Store (CDS)*. https://doi.org/10.24381/cds.adbb2d47

Dodd, P. A., Buckley, S., Campbell, K., Chierici, M., Divine, D., Eggen, V., et al. (2022). CTD profiles from NPI cruise AO-2022 across the Nansen and Amundsen Basins of the Arctic Ocean and core parameters measured from niskin bottle samples [Dataset]. *Norwegian Polar Institute*. https://doi.org/10.21334/NPOLAR.2022.D1E609E2

Dodd, P. A., Nikolopoulos, A., Buckley, S., Campbell, K., Divine, D., Eggen, V., & Fransson, A. (2022). Arctic Ocean 2022 cruise report. https://hdl.handle.net/11250/3013026

Dodd, P. A., Rabe, B., Hansen, E., Falck, E., Mackensen, A., Rohling, E., et al. (2012). The freshwater composition of the Fram Strait outflow derived from a decade of tracer measurements. *Journal of Geophysical Research*, *117*(C11). https://doi.org/10.1029/2012JC008011

Flores, H., Veyssière, G., Castellani, G., Wilkinson, J., Hoppmann, M., Karcher, M., et al. (2023). Sea-ice decline could keep zooplankton deeper for longer. *Nature Climate Change*, *13*(10), 1122–1130. https://doi.org/10.1038/s41558-023-01779-1

Gardner, W. D., Richardson, M. J., Mishonov, A. V., Lam, P. J., & Xiang, Y. (2022). Distribution, sources, and dynamics of particulate matter along trans-Arctic sections. *Journal of Geophysical Research: Oceans*, *127*(6), e2021JC017970. https://doi.org/10.1029/2021JC017970

Gonçalves-Araujo, R., Rabe, B., Peeken, I., & Bracher, A. (2018). High colored dissolved organic matter (CDOM) absorption in surface waters of the central-eastern Arctic Ocean: Implications for biogeochemistry and ocean color algorithms. *PLoS One*, *13*(1), e0190838. https://doi.org/10.1371/journal.pone.0190838

Granskog, M. A., Pavlov, A. K., Sagan, S., Kowalczuk, P., Raczkowska, A., & Stedmon, C. A. (2015). Effect of sea-ice melt on inherent optical properties and vertical distribution of solar radiant heating in Arctic surface waters. *Journal of Geophysical Research: Oceans*, *120*(10), 7028–7039. https://doi.org/10.1002/2015JC011087

Häfker, N. S., Connan-McGinty, S., Hobbs, L., McKee, D., Cohen, J. H., & Last, K. S. (2022). Animal behavior is central in shaping the realized diel light niche. *Communications Biology*, *5*(1), 562. https://doi.org/10.1038/s42003-022-03472-z

Haine, T. W., Curry, B., Gerdes, R., Hansen, E., Karcher, M., Lee, C., et al. (2015). Arctic freshwater export: Status, mechanisms, and prospects. *Global and Planetary Change*, *125*, 13–35. https://doi.org/10.1016/j.gloplacha.2014.11.013

Hersbach, H., Bell, B., Berrisford, P., Hirahara, S., Horányi, A., Muñoz-Sabater, J., et al. (2020). The ERA5 global reanalysis. *Quarterly Journal of the Royal Meteorological Society*, *146*(730), 1999–2049. https://doi.org/10.1002/qj.3803

Hill, V. J. (2008). Impacts of chromophoric dissolved organic material on surface ocean heating in the Chukchi Sea. *Journal of Geophysical Research*, *113*(C7). https://doi.org/10.1029/2007JC004119

Hoppe, C. J., Fuchs, N., Notz, D., Anderson, P., Assmy, P., Berge, J., et al. (2024). Photosynthetic light requirement near the theoretical minimum detected in Arctic microalgae. *Nature Communications*, *15*(1), 7385. https://doi.org/10.1038/s41467-024-51636-8

Horvat, C., Jones, D. R., Iams, S., Schroeder, D., Flocco, D., & Feltham, D. (2017). The frequency and extent of sub-ice phytoplankton blooms in the Arctic Ocean. *Science Advances*, *3*(3), e1601191. https://doi.org/10.1126/sciadv.1601191

Hüppe, L., Payton, L., Last, K., Wilcockson, D., Ershova, E., & Meyer, B. (2020). Evidence for oscillating circadian clock genes in the copepod Calanus finmarchicus during the summer solstice in the high Arctic. *Biology Letters*, *16*(7), 20200257. https://doi.org/10.1098/rsbl.2020.0257

Ingvaldsen, R. B., Eriksen, E., Gjøsæter, H., Engås, A., Schuppe, B. K., Assmann, K. M., et al. (2023). Under-ice observations by trawls and multi-frequency acoustics in the Central Arctic Ocean reveals abundance and composition of pelagic fauna. *Scientific Reports*, *13*(1), 1000. https://doi.org/10.1038/s41598-023-27957-x

Jahn, A., Holland, M. M., & Kay, J. E. (2024). Projections of an ice-free Arctic Ocean. *Nature Reviews Earth & Environment*, *5*(3), 164–176. https://doi.org/10.1038/s43017-023-00515-9

Kipp, L. E., Charette, M. A., Moore, W. S., Henderson, P. B., & Rigor, I. G. (2018). Increased fluxes of shelf-derived materials to the central Arctic Ocean. *Science Advances*, *4*(1), eaao1302. https://doi.org/10.1126/sciadv.aao1302

Kowalczuk, P., Sagan, S., Makarewicz, A., Meler, J., Borzycka, K., Zabłocka, M., et al. (2019). Bio-optical properties of surface waters in the Atlantic Water inflow region off Spitsbergen (Arctic Ocean). *Journal of Geophysical Research: Oceans*, *124*(3), 1964–1987. https://doi.org/10.1029/2018JC014529

Krumpen, T., Belter, H. J., Boetius, A., Damm, E., Haas, C., Hendricks, S., et al. (2019). Arctic warming interrupts the Transpolar Drift and affects long-range transport of sea ice and ice-rafted matter. *Scientific Reports*, *9*(1), 5459. https://doi.org/10.1038/s41598-019-41456-y

Last, K. S., Hobbs, L., Berge, J., Brierley, A. S., & Cottier, F. (2016). Moonlight drives ocean-scale mass vertical migration of zooplankton during the Arctic winter. *Current Biology*, *26*(2), 244–251. https://doi.org/10.1016/j.cub.2015.11.038

Laukert, G., Bauch, D., Rabe, B., Krumpen, T., Damm, E., Kienast, M., et al. (2025). Dynamic ice–ocean pathways along the transpolar drift amplify the dispersal of Siberian matter. *Nature Communications*, *16*(1), 3172. https://doi.org/10.1038/s41467-025-57881-9

Lavergne, T., Sørensen, A. M., Kern, S., Tonboe, R., Notz, D., Aaboe, S., et al. (2019). Version 2 of the EUMETSAT OSI SAF and ESA CCI sea-ice concentration climate data records. *The Cryosphere*, *13*(1), 49–78. https://doi.org/10.5194/tc-13-49-2019

Light, B., Perovich, D. K., Webster, M. A., Polashenski, C., & Dadic, R. (2015). Optical properties of melting first-year Arctic sea ice. *Journal of Geophysical Research: Oceans*, *120*(11), 7657–7675. https://doi.org/10.1002/2015JC011163

Liguori, B. T., Ehlert, C., Nöthig, E. M., van Ooijen, J. C., & Pahnke, K. (2021). The transpolar drift influence on the Arctic Ocean silicon cycle. *Journal of Geophysical Research: Oceans*, *126*(11), e2021JC017352. https://doi.org/10.1029/2021JC017352

Lowry, K. E., Pickart, R. S., Selz, V., Mills, M. M., Pacini, A., Lewis, K. M., et al. (2018). Under-ice phytoplankton blooms inhibited by spring convective mixing in refreezing leads. *Journal of Geophysical Research: Oceans*, *123*(1), 90–109. https://doi.org/10.1002/2016JC012575

Lund-Hansen, L. C., Markager, S., Hancke, K., Stratmann, T., Rysgaard, S., Ramløv, H., & Sorrell, B. K. (2015). Effects of sea-ice light attenuation and CDOM absorption in the water below the Eurasian sector of central Arctic Ocean (>88 N). *Polar Research*, *34*(1), 23978. https://doi.org/10.3402/polar.v34.23978

Massicotte, P., Babin, M., Fell, F., Fournier-Sicre, V., & Doxaran, D. (2023). The coastal surveillance through observation of ocean color (COAST ℓ OOC) dataset. *Earth System Science Data*, *15*(8), 3529–3545. https://doi.org/10.5194/essd-15-3529-2023

Massicotte, P., Babin, M., Fell, F., Fournier-Sicre, V., & Doxaran, D. (2023b). The COASTlOOC dataset [Dataset]. *SEANOE*. https://doi.org/10.17882/93570

Matsuoka, A., Hill, V., Huot, Y., Babin, M., & Bricaud, A. (2011). Seasonal variability in the light absorption properties of western Arctic waters: Parameterization of the individual components of absorption for ocean color applications. *Journal of Geophysical Research*, *116*(C2), C02007. https://doi.org/10.1029/2009JC005594

Mobley, C. D., Chai, F., Xiu, P., & Sundman, L. K. (2015). Impact of improved light calculations on predicted phytoplankton growth and heating in an idealized upwelling-downwelling channel geometry. *Journal of Geophysical Research: Oceans*, *120*(2), 875–892. https://doi.org/10.1002/2014JC010588

Moore, C. C., Bruce, E. J., Pegau, W. S., & Weidemann, A. D. (1997). WET labs ac-9: Field calibration protocol, deployment techniques, data processing, and design improvements. In *Ocean Optics XIII* (Vol. 2963, pp. 725–730).

Neeley, A. R., & Mannino, A. (2018). Ocean optics and biogeochemistry protocols for satellite ocean colour sensor validation. In *Inherent optical property measurements and protocols: Absorption coefficient* (Vol. 1.0). https://doi.org/10.25607/OBP-119

Nicolaus, M., Katlein, C., Maslanik, J., & Hendricks, S. (2012). Changes in Arctic sea ice result in increasing light transmittance and absorption. *Geophysical Research Letters*, *39*(24). https://doi.org/10.1029/2012GL053738

Park, J. Y., Kug, J. S., Bader, J., Rolph, R., & Kwon, M. (2015). Amplified Arctic warming by phytoplankton under greenhouse warming. *Proceedings of the National Academy of Sciences*, *112*(19), 5921–5926. https://doi.org/10.1073/pnas.1416884112

Pavlov, A. K., Taskjelle, T., Kauko, H. M., Hamre, B., Hudson, S. R., Assmy, P., et al. (2017). Altered inherent optical properties and estimates of the underwater light field during an Arctic under-ice bloom of Phaeocystis pouchetii. *Journal of Geophysical Research: Oceans*, *122*(6), 4939–4961. https://doi.org/10.1002/2016JC012471

Pefanis, V., Losa, S. N., Losch, M., Janout, M. A., & Bracher, A. (2020). Amplified Arctic surface warming and sea ice loss due to phytoplankton and colored dissolved material. *Geophysical Research Letters*, *47*(21), e2020GL088795. https://doi.org/10.1029/2020GL088795

Pegau, W. S. (2002). Inherent optical properties of the central Arctic surface waters. *Journal of Geophysical Research*, *107*(C10). https://doi.org/10.1029/2000JC000382

Petit, T., Hamre, B., Sandven, H., Röttgers, R., Kowalczuk, P., Zablocka, M., & Granskog, M. A. (2022). Inherent optical properties of dissolved and particulate matter in an Arctic fjord (Storfjorden, Svalbard) in early summer. *Ocean Science*, *18*(2), 455–468. https://doi.org/10.5194/os-18-455-2022

Pope, R. M., & Fry, E. S. (1997). Absorption spectrum (380–700 nm) of pure water. II. Integrating cavity measurements. *Applied Optics*, *36*(33), 8710–8723. https://doi.org/10.1364/AO.36.008710

Randelhoff, A., Lacour, L., Marec, C., Leymarie, E., Lagunas, J., Xing, X., et al. (2020). Arctic mid-winter phytoplankton growth revealed by autonomous profilers. *Science Advances*, *6*(39), eabc2678. https://doi.org/10.1126/sciadv.abc2678

Rantanen, M., Karpechko, A. Y., Lipponen, A., Nordling, K., Hyvärinen, O., Ruosteenoja, K., et al. (2022). The Arctic has warmed nearly four times faster than the globe since 1979. *Communications Earth & Environment*, *3*(1), 168. https://doi.org/10.1038/s43247-022-00498-3

Renaud, P. E., Daase, M., Leu, E., Geoffroy, M., Basedow, S., Inall, M., et al. (2024). Extreme mismatch between phytoplankton and grazers during Arctic spring blooms and consequences for the pelagic food-web. *Progress in Oceanography*, *229*, 103365. https://doi.org/10.1016/j.pocean.2024.103365

Reynolds, R. A., Stramski, D., & Neukermans, G. (2016). Optical backscattering by particles in Arctic seawater and relationships to particle mass concentration, size distribution, and bulk composition. *Limnology and Oceanography*, *61*(5), 1869–1890. https://doi.org/10.1002/lno.10341

Rijkenberg, M. J., Slagter, H. A., Rutgers van der Loeff, M., Van Ooijen, J., & Gerringa, L. J. (2018). Dissolved Fe in the deep and upper Arctic Ocean with a focus on Fe limitation in the Nansen Basin. *Frontiers in Marine Science*, *5*, 88. https://doi.org/10.3389/fmars.2018.00088

Röttgers, R., Doxaran, D., & Dupouy, C. (2016). Quantitative filter technique measurements of spectral light absorption by aquatic particles using a portable integrating cavity absorption meter (QFT-ICAM). *Optics Express*, *24*(2), A1–A20. https://doi.org/10.1364/OE.24.0000A1

Röttgers, R., & Gehnke, S. (2012). Measurement of light absorption by aquatic particles: Improvement of the quantitative filter technique by use of an integrating sphere approach. *Applied Optics*, *51*(9), 1336–1351. https://doi.org/10.1364/AO.51.001336

Röttgers, R., McKee, D., & Woźniak, S. B. (2013). Evaluation of scatter corrections for ac-9 absorption measurements in coastal waters. *Methods in Oceanography*, *7*, 21–39. https://doi.org/10.1016/j.mio.2013.11.001

Sakshaug, E., & Slagstad, D. A. G. (1991). Light and productivity of phytoplankton in polar marine ecosystems: A physiological view. *Polar Research*, *10*(1), 69–86. https://doi.org/10.3402/polar.v10i1.6729

Sandven, H., Gonçalves-Araujo, R., Röttgers, R., Granskog, M. A., & Hamre, B. (2026). Colored dissolved organic matter (CDOM) and particulate absorption coefficients of sea water in the Central Arctic Ocean: NPI cruise AO-2022 (2022710) [Dataset]. *Norwegian Polar Institute*. https://doi.org/10.21334/NPOLAR.2026.89553850

Sandven, H., Granskog, M. A., & Hamre, B. (2026). In situ spectral beam attenuation and absorption coefficients of sea water in the western Amundsen and Nansen basins: NPI cruise AO-2022 (2022710) [Dataset]. *Norwegian Polar Institute*. https://doi.org/10.21334/NPOLAR.2025.1ED859A1

Sandven, H., Granskog, M. A., Opdal, A. F., Connan-McGinty, S., Hamre, B., & McKee, D. (2025). Increased light availability in the northern Barents Sea driven by sea ice loss. *Journal of Geophysical Research: Oceans*, *130*(6), e2025JC022370. https://doi.org/10.1029/2025JC022370

Sandven, H., Hamre, B., Petit, T., Röttgers, R., Liu, H., & Granskog, M. A. (2023). Seasonality and drivers of water column optical properties on the northwestern Barents Sea shelf. *Progress in Oceanography*, *217*, 103076. https://doi.org/10.1016/j.pocean.2023.103076

Sandven, H., Kristoffersen, A. S., Chen, Y. C., & Hamre, B. (2020). In situ measurements of the volume scattering function with LISST-VSF and LISST-200X in extreme environments: Evaluation of instrument calibration and validity. *Optics Express*, *28*(25), 37373–37396. https://doi.org/10.1364/OE.411177

Sandven, H., McKee, D., Gonçalves-Araujo, R., Röttgers, R., Opdal, A. F., Assmy, P., & Granskog, M. (2026). Supporting data for terrestrial runoff divides the Central Arctic Ocean and shapes the biologically relevant marine lightscape (version v2) [Dataset]. *Zenodo*. https://doi.org/10.5281/zenodo.18669082

Schartmüller, B., Anderson, P., McKee, D., Connan-McGinty, S., Kopec, T. P., Daase, M., et al. (2023). Development and calibration of a high dynamic range and autonomous ocean-light instrument to measure sub-surface profiles in ice-covered waters. *Applied Optics*, *62*(31), 8308–8315. https://doi.org/10.1364/AO.502437

Schlitzer, R. (2022). Ocean data view. http://www.odw.awi.de

Sherr, E. B., Sherr, B. F., Wheeler, P. A., & Thompson, K. (2003). Temporal and spatial variation in stocks of autotrophic and heterotrophic microbes in the upper water column of the central Arctic Ocean. *Deep Sea Research Part I: Oceanographic Research Papers*, *50*(5), 557–571. https://doi.org/10.1016/S0967-0637(03)00031-1

Smith, R. C. (1973). Optical properties of the Arctic upper water. *Arctic*, *26*(4), 303–313. https://doi.org/10.14430/arctic2929

Soja-Woźniak, M., Holtrop, T., Woutersen, S., vander Woerd, H. J., Lund-Hansen, L. C., & Huisman, J. (2025). Loss of sea ice alters light spectra for aquatic photosynthesis. *Nature Communications*, *16*(1), 4059. https://doi.org/10.1038/s41467-025-59386-x

Stedmon, C. A., Amon, R. M., Bauch, D., Bracher, A., Gonçalves-Araujo, R., Hoppmann, M., et al. (2021). Insights into water mass origins in the central Arctic Ocean from in-situ dissolved organic matter fluorescence. *Journal of Geophysical Research: Oceans*, *126*(7), e2021JC017407. https://doi.org/10.1029/2021JC017407

Stedmon, C. A., Amon, R. M. W., Rinehart, A. J., & Walker, S. A. (2011). The supply and characteristics of colored dissolved organic matter (CDOM) in the Arctic Ocean: Pan Arctic trends and differences. *Marine Chemistry*, *124*(1–4), 108–118. https://doi.org/10.1016/j.marchem.2010.12.007

Stedmon, C. A., Granskog, M. A., & Dodd, P. A. (2015). An approach to estimate the freshwater contribution from glacial melt and precipitation in East Greenland shelf waters using colored dissolved organic matter (CDOM). *Journal of Geophysical Research: Oceans*, *120*(2), 1107–1117. https://doi.org/10.1002/2014JC010501

Stroeve, J., Vancoppenolle, M., Veyssiere, G., Lebrun, M., Castellani, G., Babin, M., et al. (2021). A multi-sensor and modeling approach for mapping light under sea ice during the ice-growth season. *Frontiers in Marine Science*, *7*, 592337. https://doi.org/10.3389/fmars.2020.592337

Sverdrup, H. U. (1953). On conditions for the vernal blooming of phytoplankton. *Journal du Conseil Int. Explor. Mer*, *18*(3), 287–295. https://doi.org/10.1093/icesjms/18.3.287

Tremblay, J. É., Anderson, L. G., Matrai, P., Coupel, P., Bélanger, S., Michel, C., & Reigstad, M. (2015). Global and regional drivers of nutrient supply, primary production and CO2 drawdown in the changing Arctic Ocean. *Progress in Oceanography*, *139*, 171–196. https://doi.org/10.1016/j.pocean.2015.08.009

Utne-Palm, A. C. (1999). The effect of prey mobility, prey contrast, turbidity and spectral composition on the reaction distance of Gobiusculus flavescens to its planktonic prey. *Journal of Fish Biology*, *54*(6), 1244–1258. https://doi.org/10.1111/j.1095-8649.1999.tb02052.x

Werdell, P. J., & Bailey, S. W. (2005). An improved in-situ bio-optical data set for ocean color algorithm development and satellite data product validation. *Remote Sensing of Environment*, *98*(1), 122–140. https://doi.org/10.1016/j.rse.2005.07.001

Wilson, Aksenov, Y., Rynders, S., Kelly, S. J., Krumpen, T., & Coward, A. C. (2021). Significant variability of structure and predictability of Arctic Ocean surface pathways affects basin-wide connectivity. *Communications Earth & Environment*, *2*(1), 164. https://doi.org/10.1038/s43247-021-00237-0

Wünsch, U. J., Gonçalves-Araujo, R., Granskog, M. A., Gry Ebbesen, L., Papadimitraki, M., & Stedmon, C. A. (2025). Fluorescence as a tracer of the susceptibility of dissolved organic matter to photodegradation in the Arctic Ocean. *Limnology and Oceanography*, *70*(8), 2299–2314. https://doi.org/10.1002/lno.70119

Zhang, J., & Rothrock, D. A. (2003). Modeling global sea ice with a thickness and enthalpy distribution model in generalized curvilinear coordinates. *Monthly Weather Review*, *131*(5), 845–861. https://doi.org/10.1175/1520-0493(2003)131<0845:mgsiwa>2.0.co;2

References From the Supporting Information

Epstein, S., & Mayeda, T. (1953). Variation of O18 content of waters from natural sources. *Geochimica et Cosmochimica Acta*, *4*(5), 213–224. https://doi.org/10.1016/0016-7037(53)90051-9

Holm-Hansen, O., & Riemann, B. (1978). Chlorophyll a determination: Improvements in methodology. *Oikos*, *30*(3), 438–447. https://doi.org/10.2307/3543338

Lefering, I., Röttgers, R., Weeks, R., Connor, D., Utschig, C., Heymann, K., & McKee, D. (2016). Improved determination of particulate absorption from combined filter pad and PSICAM measurements. *Optics Express*, *24*(22), 24805–24823. https://doi.org/10.1364/OE.24.024805

Roesler, C., Uitz, J., Claustre, H., Boss, E., Xing, X., Organelli, E., et al. (2017). Recommendations for obtaining unbiased chlorophyll estimates from in situ chlorophyll fluorometers: A global analysis of WET labs ECO sensors. *Limnology and Oceanography: Methods*, *15*(6), 572–585. https://doi.org/10.1002/lom3.10185

Stramski, D., Reynolds, R. A., Kaczmarek, S., Uitz, J., & Zheng, G. (2015). Correction of pathlength amplification in the filter-pad technique for measurements of particulate absorption coefficient in the visible spectral region. *Applied Optics*, *54*(22), 6763–6782. https://doi.org/10.1364/AO.54.006763

Sundfjord, A., Assmann, K. M., Lundesgaard, Ø., Renner, A. H., Lind, S., & Ingvaldsen, R. B. (2020). Suggested water mass definitions for the central and northern Barents Sea, and the adjacent Nansen Basin: Workshop Report. *The Nansen Legacy Report Series*, *8*. https://doi.org/10.7557/nlrs.5707